PHILOSOPHICAL TRANSACTIONS A

royalsocietypublishing.org/journal/rsta

Research

Cite this article: Ryvkin M, Slesarenko V, Cherkaev A, Rudykh S. 2019 Fault-tolerant elastic–plastic lattice material. *Phil. Trans. R. Soc. A* **378**: 20190107.
http://dx.doi.org/10.1098/rsta.2019.0107

Accepted: 22 July 2019

One contribution of 12 to a theme issue 'Modelling of dynamic phenomena and localization in structured media (part 2)'.

Subject Areas:
mechanical engineering, materials science, mathematical modelling, applied mathematics

Keywords:
fault tolerance, elastic–plastic lattice, design of inhomogeneous lattice, experimental date of failure, stages of destruction

Author for correspondence:
Andrej Cherkaev
e-mail: cherk@math.utah.edu

Fault-tolerant elastic–plastic lattice material

Michael Ryvkin[1], Viacheslav Slesarenko[2,3], Andrej Cherkaev[4] and Stephan Rudykh[5]

[1]School of Mechanical Engineering, Tel Aviv University, Ramat Aviv 69978, Israel
[2]Faculty of Aerospace Engineering, Technion, Haifa, Israel
[3]Lavrentyev Institute of Hydrodynamics SB RAS, Novosibirsk, 630090, Russia
[4]Department of Mathematics, University of Utah, Salt Lake City, UT 94112, USA
[5]Department of Mechanical Engineering, University of Wisconsin–Madison, Madison, WI, USA

AC, 0000-0001-7824-445X; SR, 0000-0002-4568-8326

The paper describes a fault-tolerant design of a special two-dimensional beam lattice. The morphology of such lattices was suggested in the theoretical papers (Cherkaev and Ryvkin 2019 *Arch. Appl. Mech.* **89**, 485–501; Cherkaev and Ryvkin 2019 *Arch. Appl. Mech.* **89**, 503–519), where its superior properties were found numerically. The proposed design consists of beam elements with two different thicknesses; the lattice is macro-isotropic and stretch dominated. Here, we experimentally verify the fault-tolerant properties of these lattices. The specimens were three-dimensional-printed from the VeroWhite elastoplastic material. The lattice is subjected to uniaxial tensile loading. Due to its morphology, the failed beams are evenly distributed in the lattice at the initial stage of damage; at this stage, the material remains intact, preserves its bearing ability, and supports relatively high strains before the final failure. At the initial phase of damage, the thinner beams buckle; then another group of separated thin beams plastically yield and rupture. The fatal macro-crack propagates after the distributed damage reaches a critical level. This initial distributed damage stage allows for a better energy absorption rate before the catastrophic failure of the structure. The experimental results are supported by simulations which confirm that the proposed fault-tolerant material possesses excellent energy absorption properties thanks to the distributed damage stage phenomenon.

© 2019 The Author(s) Published by the Royal Society. All rights reserved.

THE ROYAL SOCIETY PUBLISHING

Downloaded from royalsocietypublishing.org/rsta/article-pdf/doi/10.1098/rsta.2019.0107/1316862/rsta.2019.0107.pdf
by University Freiburg user
on 04 November 2026

This article is part of the theme issue 'Modelling of dynamic phenomena and localization in structured media (part 2)'.

1. Introduction

The majority of engineering materials fail due to cracking. A catastrophic macro-crack propagates through a homogeneous specimen subjected to uniform tensile loading. In both cases of brittle as well as ductile materials, the crack propagates due to strain localization. We design and experimentally test a fault-tolerant material that resists crack propagation: the damage develops slowly, and the strain localization stage is preceded by a phase where damage is evenly distributed in the material volume. Consequently, the specimen remains intact while experiencing large irreversible deformations and large energy dissipation. The prominent examples of natural fault-tolerant materials with the distributed damage stage are bone tissues [1,2] and nacre [3]. The fault tolerance response in these materials is thanks to their specific microstructure. They possess sacrificial links [4,5] or soft interfaces [6–8], which fail first, while the material remains intact at a macro scale. Similarly, some polymer materials possess distributed sacrificial links, failure of which does not destroy the material's integrity [9].

Fault (damage) tolerant materials are of significant interest to modern engineering practices [10]. Non-localized distributed damage stage materials are especially beneficial because they allow monitoring of the structural health of the material and detecting damage before fatal collapse [11].

A one-dimensional structural illustration of the idea of sacrificial links was presented in [12], where after partial damage of sacrificial rods, the loading was carried by the initially inactive curved rods called 'waiting links'. Dynamics and waves of damage in a chain with sacrificial links are described in [13,14]. Activation of these rods in a partially damaged structure increases the local stiffness and leads to distributed damage and damage waves. The dynamics of damage was numerically investigated in the paper [15]. Rational design of the elements of such structures against waves of damage was investigated in [16]. A helicoidal structure with increasing energy absorption was suggested in [17]. The designs of impact-protecting structures with waiting links were described in [18,19].

The waiting links are not initially activated, which reduces the stiffness of an undamaged structure. In [20,21], another approach is used. All beams in the lattice are initially active and resist the load, but some of them are broken if the external load exceeds a threshold, which creates distributed patterns of localized damage. In [21], the design of a two-dimensional material with the microstructure providing the fault-tolerant response for a biaxial tension was suggested and numerically tested. The superior fracture toughness was achieved by redistributing the material between links, resulting in the periodic heterogeneous beam lattice (bi-lattice) consisting of beams with different thicknesses. The resulting uneven stresses in neighbouring elements lead to many isolated faults that do not grow into cracks during the first stage of damage but consume significant impact energy.

The primary goal of the present work is to get an experimental verification of the theoretical results obtained in [21]. The experiment is performed for slightly different boundary conditions than in that theoretical paper, and the parent material is not brittle, but the arrangement of thin sacrificial elements is the same. The expected result, fault tolerance of the specimen, is observed in the experiment. This result provides evidence that the design concept developed in [21] is robust; one might expect this because the concept is geometrical and could apply to various materials.

2. The theoretical result for the bi-axial tension of brittle lattice

The design of a heterogeneous brittle fault-tolerant lattice, which was found in [21] is presented in figure 1. This lattice (bi-lattice) is a superposition of two basic lattices (figure 1*c*) with different

Downloaded from royalsocietypublishing.org/rsta/article-pdf/doi/10.1098/rsta.2019.0107/1316862/rsta.2019.0107.pdf
by University Freiburg user
on 04 November 2026

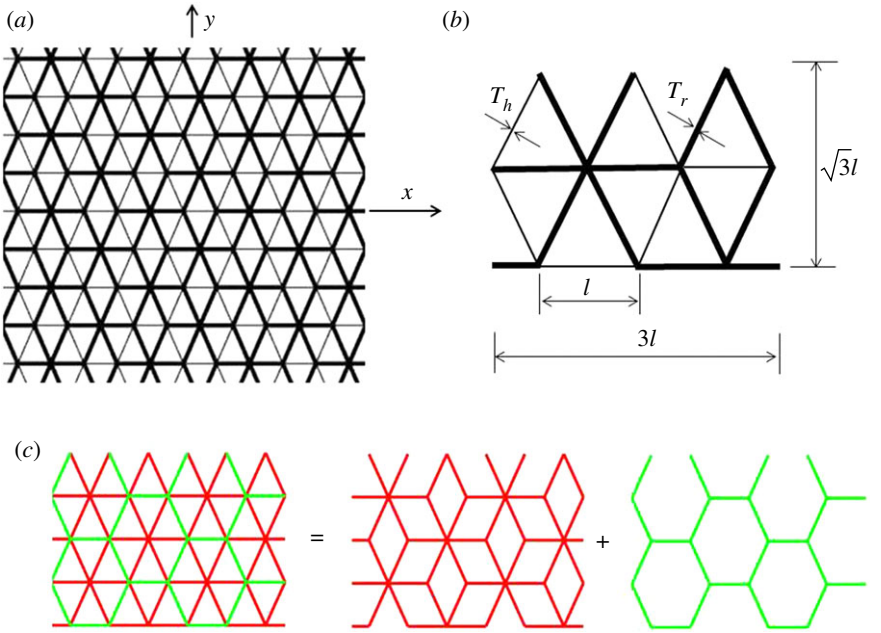


Figure 1. Heterogeneous fault-tolerant beam lattice (*a*), its repetitive cell (*b*). The lattice structure is a combination of rhombille and hexagonal lattices (*c*). (Online version in colour.)

thicknesses of the beams. The bi-lattice is isotropic due to the elastic symmetry of the periodicity cell, and its effective Young modulus and Poisson ratio are analytically calculated (see appendix). Although both rhombille and hexagonal lattices are bending dominated, their combination in the bi-lattice is stretch dominated; and, therefore, its stiffness is an order of magnitude higher than the stiffness of each of the constituents. Nevertheless, the stiffness of bi-lattice is smaller than the stiffness of a regular triangular lattice, but its fault tolerance is much higher. In the uniform triangular lattice, the failure of one of the links initiates the failure of its neighbours, and a straight linear crack is formed [20,22]. The heterogeneous bi-lattice is fault tolerant because its damage is distributed through the volume; the local damage starts and is arrested; then it starts in another place, and so on.

The parameters of the bi-lattice are as follows: the rhombille lattice consists of beams with thickness T_r called *r*-beams, and a hexagonal lattice composed of beams with thickness T_h called *h*-beams. We found by simulation that in better designs $T_h < T_r$. The ratio of these thicknesses is called τ, ($\tau = T_h/T_r < 1$). The relative density of cellular lattice material ρ is defined as the ratio of parent material volume in the repetitive periodic cell to the total cell volume. For the considered bi-lattice

$$\rho = \frac{2}{\sqrt{3}}(t_h + 2t_r), \tag{2.1}$$

where $t_h = T_h/l$ and $t_r = T_r/l$ are the non-dimensional beam thicknesses normalized by the elements length l. The lattice was subjected to elongation in one direction; the average strain in the perpendicular direction was fixed. These conditions correspond to the bi-axial tension.

Two failure criteria were considered, the maximal stress criterion and the rheological criterion, which take into account the prehistories of previous loadings that may have weakened the beam. Initially, one beam was removed; at each of the next steps, another beam was removed. The maximum stress criterion requires removing the beam with the highest skin stress σ_s. The rheological criterion assumes that all overloaded beams lose some of their strength; the reduced critical stress of these beams is recalculated after each step and the beam with the highest reduced stress is removed. The value of the maximal skin stress in each beam is calculated as a sum of

Downloaded from royalsocietypublishing.org/rsta/article-pdf/doi/10.1098/rsta.2019.0107/1316862/rsta.2019.0107.pdf
by University Freiburg user
on 04 November 2026

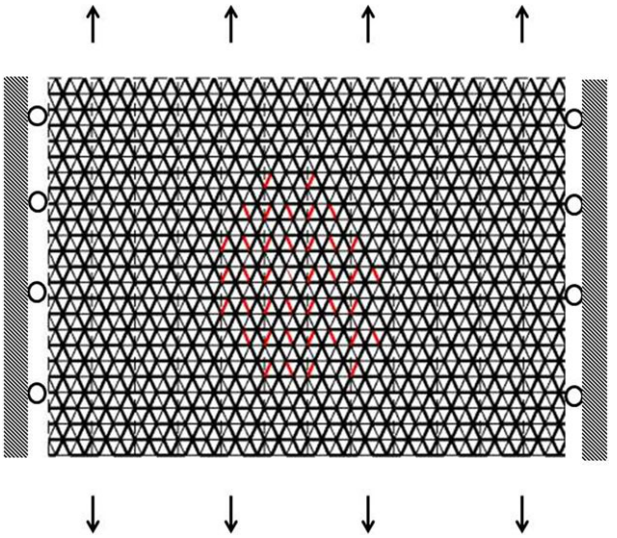


Figure 2. Damage pattern for the brittle fault-tolerant bi-lattice. The broken rods are shown in red. (Online version in colour.)

the bending stress caused by a maximal bending moment M, which is approached at one of its extremities, and the stress caused by an axial force N

$$\sigma_s = \left|\frac{MT}{2I}\right| + \frac{N}{A}, \tag{2.2}$$

where T is the thickness of the beam cross section, A is the cross-section area and I its moment of inertia.

The damage propagation in the bi-lattice of relative density $\rho = 0.1155$ with different beam thickness ratios τ was numerically simulated, and it was found that the most pronounced fault tolerance effect takes place for $\tau = 0.25$. The pattern of distributed damage for both failure criteria after 40 consecutive breakages was the same; it is presented in figure 2.

3. The experiment

(a) Choice of the parameters

The analysis of damage propagation in the heterogeneous lattice subjected to a uniaxial tension is carried out in the same way as in [21] for other boundary conditions. A rectangular lattice domain includes $12 \times 12 = 144$ repetitive cells; their morphology is shown in figure 1*b*. Beam elements of length l are rigidly connected at the nodal points, each node has two translational and one rotational degree of freedom. The elastic response of an element in the local beam related coordinate system is described by the stiffness matrix $K_e[6 \times 6]$, e.g. [23]

$$K_e = \frac{EI}{l^3}\begin{bmatrix} \beta & 0 & 0 & -\beta & 0 & 0 \\ 0 & 12 & 6l & 0 & -12 & 6l \\ 0 & 6l & 4l^2 & 0 & -6l & 2l^2 \\ -\beta & 0 & 0 & \beta & 0 & 0 \\ 0 & -12 & -6l & 0 & 12 & -6l \\ 0 & 6l & 4l^2 & 0 & -6l & 4l^2 \end{bmatrix}, \tag{3.1}$$

where E_p is the parent material Young modulus and $\beta = Al^2/I$ is the square of beam slenderness ratio. The analysis of the rectangular domain was carried out by the use of the representative cell method [24]. This method is based on the discrete Fourier transform, it allows for replacing the analysis of a whole domain by the analysis of the single repetitive cell consisting of 19

Downloaded from royalsocietypublishing.org/rsta/article-pdf/doi/10.1098/rsta.2019.0107/1316862/rsta.2019.0107.pdf
by University Freiburg user
on 04 November 2026

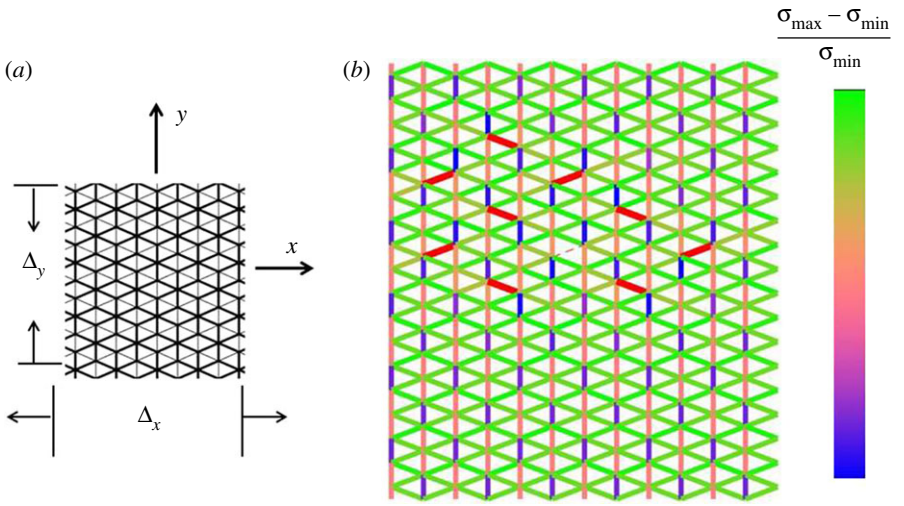


Figure 3. Uniaxial tension of fault-tolerant bi-lattice. Loading scheme (*a*) and maximal stress distribution after breakage of 10 beams denoted by red (*b*). Dashed thin red line denotes the initial flaw. (Online version in colour.)

rods (figure 1*b*). The stiffness matrix of the single cell is obtained by the standard methods of structural mechanics (e.g. [23]). The representative cell method uses the boundary conditions in the form of jumps in the displacements and tractions between the nodes at the opposite sides of the rectangular domain. The considered state of uniaxial tension in the horizontal direction is obtained by assigning the jumps in the displacements normal to the respective domain boundaries. Namely, the jump in the x-direction corresponds to the elongation Δ_x and the jump in the y-direction corresponds to the contraction $\Delta_y = -\nu_* \Delta_x$, where ν_* is the effective Poisson ratio of the heterogeneous lattice. The loading scheme is illustrated in figure 3*a*. The damage propagation is modelled by sequentially removing the broken beams following the maximal stress criterion by the use of (2.2) as is described in the previous section.

The thicknesses ratio parameter τ varies in the interval $(0, 1)$. For a sufficiently small τ, thin h-beams will fail first; however, if these beams are too thin, they do not significantly improve the overall elastic response of a remaining compliant rhombille honeycomb. The opposite case $\tau = 1$ corresponds to the triangular lattice with uniform elements, which has maximal stiffness but is not fault tolerant. The design aims to compromise these properties. Therefore, the design goal is to find a fault-tolerant lattice with a large ratio τ.

The numerical experiments have shown that for the bi-lattice material with relative density $\rho = 0.231$, the value is $\tau = 1/3$. The effective elastic properties for this layout are calculated by the formulae derived in [21] (see appendix)

$$\left.\begin{aligned} \nu_* &= 0.441 \\ \frac{E_*}{E_p} &= 0.0643 \end{aligned}\right\}, \quad \text{and} \tag{3.2}$$

where E_p is the Young modulus of the parent material. Note that the lattice ($\tau = 1$) of maximal stiffness for the same density has the Young modulus $E_*/E_p = 0.0769$, i.e. the reduction of the stiffness is only 16%. The maximal stress distribution in the lattice rods after several initial breaks is illustrated in figure 3*b*. The colour of each element represents its maximal stress, which is evaluated by (2.2); the dashed thin red line denotes the initially introduced flaw. The vertical rods perpendicular to the loading direction are subjected to a non-uniform contraction, where the h-rods are compressed more than the r-ones; the consequence is discussed in the next section.

Downloaded from royalsocietypublishing.org/rsta/article-pdf/doi/10.1098/rsta.2019.0107/1316862/rsta.2019.0107.pdf
by University Freiburg user
on 04 November 2026

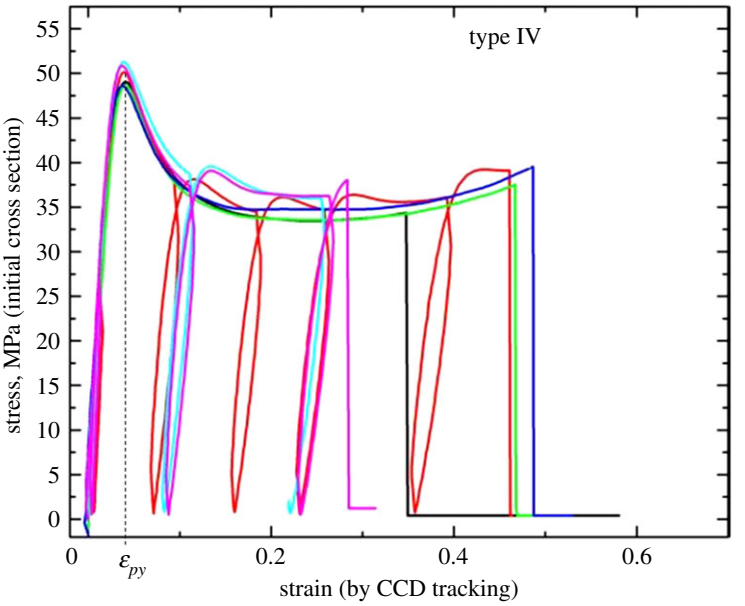


Figure 4. Uniaxial tension test for VeroWhite material with the loading/unloading. The colours of the curves denote several tests. (Online version in colour.)

(b) Materials and scheme of experiment

We prepared the heterogeneous lattice specimen from a elastic–plastic polymer material rather than from the brittle one that was considered in the theoretical analysis in [21] because this polymer material was widely available. The fault tolerance of the theoretical design is mainly due to the special geometry of the lattice and the elastic response of parent material. Therefore, it was plausible to hypothesize that the special response of the lattice is observed for a non-brittle material as well. The results presented below show that this hypothesis is validated and our concept of the design is robust and applicable to various types of materials.

The heterogeneous lattice structures were produced by a Polyjet 3D printer using the Stratasys Objet Connex 260 machine. The commercially available stiff polymeric material VeroWhite was selected for the fabrication of the specimens from the relatively broad spectrum of the printable materials [25]. Several uniaxial tests with intermediate unloading were performed on the homogeneous specimens with dimensions corresponding to ASTM D638 standard (Type IV) to verify the elastic properties of this parent material. The parent material demonstrates elastic–plastic mechanical behaviour with pronounced plastic elongation after reaching yield stress, as shown in figure 4. Intermediate unloading–loading cycles reveal slight hysteresis caused by relatively weak viscoelastic properties of the material.

The experimentally verified elastic–plastic response is characterized by the following data: Young modulus $E_p = 1650$ MPa, Poisson ratio $\nu_p = 0.42$ and yield stress $\sigma_{py} = 50$ MPa. The strain ε_{py} corresponding to the limit of the linear elastic response (figure 4) is

$$\varepsilon_{py} = \frac{\sigma_{py}}{E_p} = 0.0303. \tag{3.3}$$

The scheme of the experimental set-up is presented in figure 5. The rectangular lattice sample has length $L_x = 217$ mm in the loading direction, width $L_y = 157$ mm and out-of-plane thickness $l_o = 1.5$ mm. The structural parameters for the relative density $\rho = 0.231$ are chosen to fit the results described in the previous section: $l = 10.5$ mm, $T_h = 0.94$ mm and $T_r = 0.3$ mm (figure 1*b*). The opposite vertical boundaries of the specimen are fixed at the moving supports, and an

Downloaded from royalsocietypublishing.org/rsta/article-pdf/doi/10.1098/rsta.2019.0107/1316862/rsta.2019.0107.pdf
by University Freiburg user
on 04 November 2026

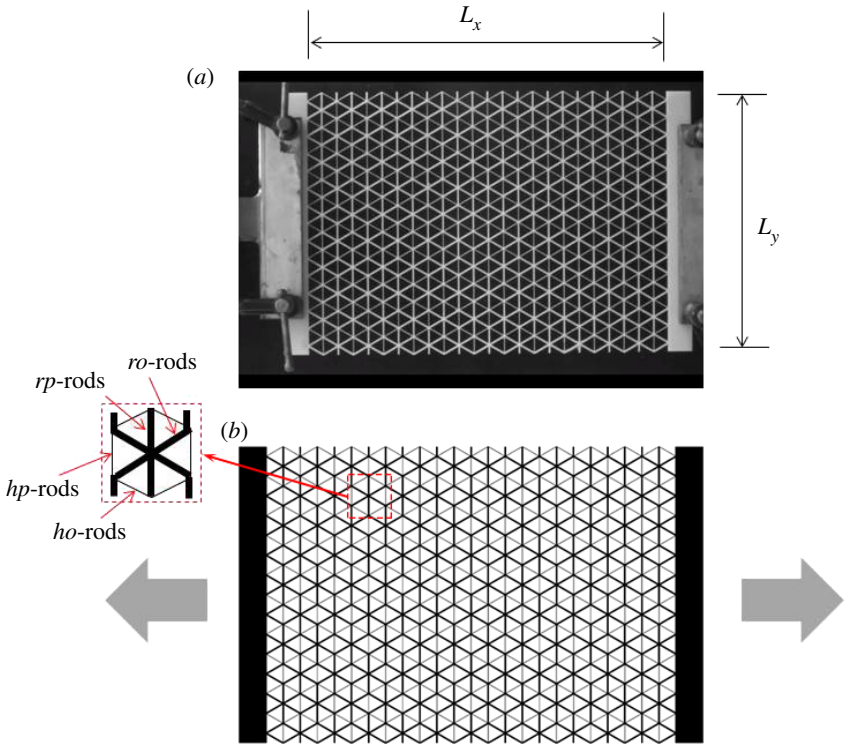


Figure 5. Experimental sample (*a*) and the loading scheme (*b*). (Online version in colour.)

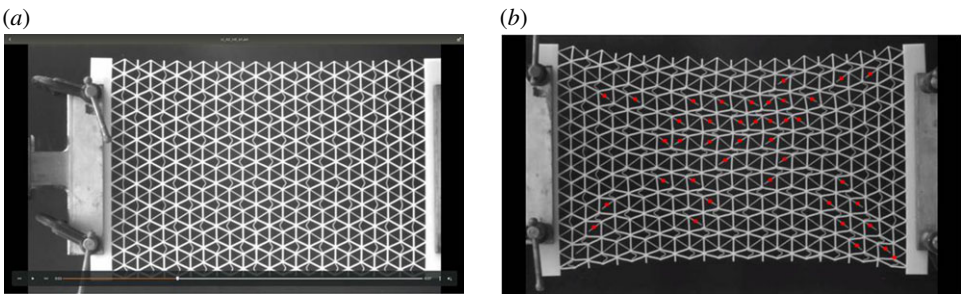


Figure 6. The stages of damage: buckling of vertical *r*-rods (*a*) and rupture of the oblique rods (*b*). (Online version in colour.)

elongation test is carried out for quasi-static conditions with the speed of support $5\,\mathrm{mm\,min^{-1}}$, which corresponds to the strain rate $3.8 \times 10^{-4}\,\mathrm{s^{-1}}$.

The material demonstrates the expected fault tolerance response with distributed damage before a macro-crack emerges. Two visually observed sequential stages with different types of damage are shown in figure 6. Red circles indicate the location of broken elements. The next section discusses the obtained results.

4. Results and discussion

(a) Distributed buckling and yielding

The nominal stress–strain diagram of the experiment is presented in figure 7. The results of two tests with and without intermediate loading–unloading are shown. For the small strains, the

Downloaded from royalsocietypublishing.org/rsta/article-pdf/doi/10.1098/rsta.2019.0107/1316862/rsta.2019.0107.pdf
by University Freiburg user
on 04 November 2026

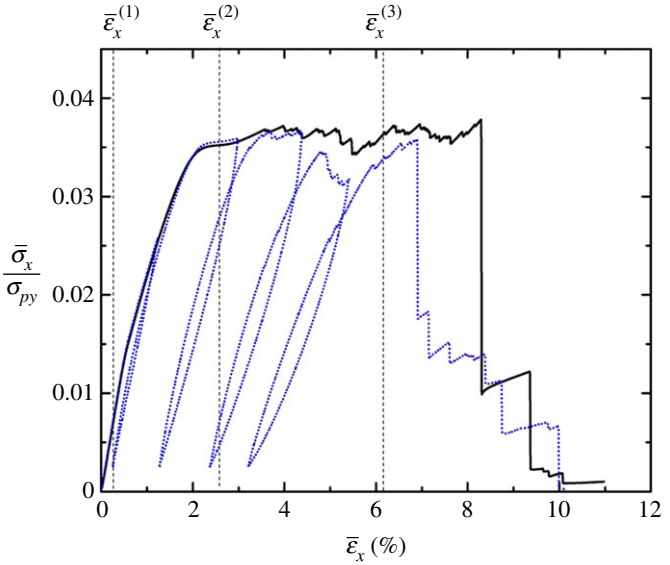


Figure 7. Stress–strain diagram of uniaxial tension in the fault-tolerant bi-lattice with and without unloading. (Online version in colour.)

lattice material is linearly elastic, and its Young modulus, which is the inclination angle of the stress–strain graph, is 0.108 GPa. This value is very close to the theoretical result calculated by (3.2) $E_* = 0.106$ GPa.

As the strain reaches a threshold[1]

$$\bar{\varepsilon}_x^1 = 0.004 \tag{4.1}$$

a material softening occurs, shown as a kink-like transition to a straight stress–strain dependence with the smaller angle. This phenomenon is presented in figure 8, which is the zoomed in part of figure 7. This behaviour is due to the buckling of the thin *h*-rods perpendicular to the loading direction; these buckled rods will be denoted as *hp*-rods (figures 5 and 6*a*). The unloading curve in figure 8 shows that the material response contains an irreversible deformation component. Hence, the elastic–plastic buckling is also considered distributed damage.

The value $\bar{\varepsilon}_x^1$ is theoretically estimated. The numerical simulation shows that for the considered parameters the axial shortening strain in the *hp*-rods has the same absolute value as the overall elongation strain

$$\varepsilon^{hp} = -\bar{\varepsilon}_x. \tag{4.2}$$

The critical value ε^{hp} is determined by the Euler buckling force for a beam with the clamped–clamped boundary conditions

$$P_E = \frac{4\pi^2 E_p I}{l^2}. \tag{4.3}$$

If the beam's cross section is rectangular, the corresponding negative buckling axial strain is given by the formula

$$\varepsilon_E^{hp} = \frac{P_E}{EA} = \frac{\pi^2}{3} t_h^2. \tag{4.4}$$

The buckling takes place when $\varepsilon^{hp} = \varepsilon_E^{hp}$; in view of (4.2), the theoretical value of $\bar{\varepsilon}_x^1$ is 0.0027. A notable discrepancy of this value from the experimental data (4.1) can be attributed to the difference in boundary conditions. Theoretical estimation is obtained for the pure periodic

[1]The bar hereafter is used to denote the average strains in the specimen obtained by the division of elongation to the initial length.

Downloaded from royalsocietypublishing.org/rsta/article-pdf/doi/10.1098/rsta.2019.0107/1316862/rsta.2019.0107.pdf
by University Freiburg user
on 04 November 2026

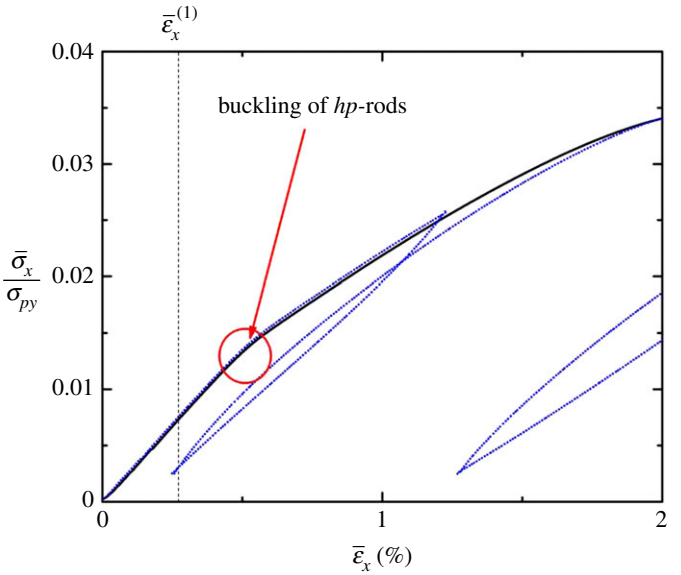


Figure 8. Zoomed in part of the bi-lattice stress–strain diagram for small strains. (Online version in colour.)

displacements field, while in the experiment the effective vertical contraction is diminished because the vertical displacements at the boundaries of the specimen parallel to the *y*-axis are clamped.

Additional experiments are conducted on the homogeneous triangular lattice with uniform elements ($T_h = T_r = T$) under uniaxial tension. In contrast to the heterogeneous bi-lattice, the buckling phenomenon was not observed. The difference in response is explained as follows: the average transverse contraction $\bar{\varepsilon}_y = -\nu_* \bar{\varepsilon}_x$ for the heterogeneous lattice is higher than for the homogeneous one due to the larger effective Poisson ratio [21]. In addition, this contraction in the heterogeneous lattice is distributed non-uniformly with higher strains at the thin *hp*-rods (figure 3*b*):

$$\bar{\varepsilon}_y = \tfrac{1}{3}(\varepsilon^{hp} + 2\varepsilon^{rp}). \tag{4.5}$$

Here, ε^{rp} is the deformation of *r*-rods perpendicular to the loading direction. Since for the thicker *rp*-rods $\varepsilon^{rp} < \varepsilon^{hp}$, from (4.5) it follows that $\varepsilon^{hp} > \bar{\varepsilon}_y$.

A plateau in the stress–strain diagram follows the linear elastic response with buckled perpendicular rods. Such a response is similar to the response of the solid parent material (figure 4); however, the underlying physical mechanism is different. For the solid material, the plastic deformation is localized in a specific material region (the neck) and is characterized by the significant stress drop at the beginning of the plateau. In the lattice, the main reason for the plateau formation is also plasticity; however, the resultant overall plastic response is a result of distributed plastic deformation followed by the rupture of multiple separated oblique *h*-rods (i.e. *ho*-rods), which explains the saw-like shape of the graph. The visual observation shows that the rupture of *ho*-rods starts at an average deformation of about $\bar{\varepsilon}_x = 0.042$, and the specimen failure accompanied by the damage localization and macro-crack appearance takes place for an average strain of 0.07.

The obtained experimental results are in agreement with the simulation. The relation between the axial strain of *ho*-rods and the overall specimen deformation is computed as $\varepsilon_{ho} = 1.16\bar{\varepsilon}_x$. So, by (3.3), the theoretical value of the deformation corresponding to the yielding of the *ho*-rods is $\bar{\varepsilon}_x^{(2)} = 0.0303/1.16 = 0.0261$, which is close to the beginning of the plateau region in the experiment. The value $\bar{\varepsilon}_x^3$ corresponding to the yielding of thick oblique *r*-rods (*ro*-rods) is significantly higher; a similar argument shows that it is about 0.061, which is consistent with the experimental data.

Downloaded from royalsocietypublishing.org/rsta/article-pdf/doi/10.1098/rsta.2019.0107/1316862/rsta.2019.0107.pdf
by University Freiburg user
on 04 November 2026

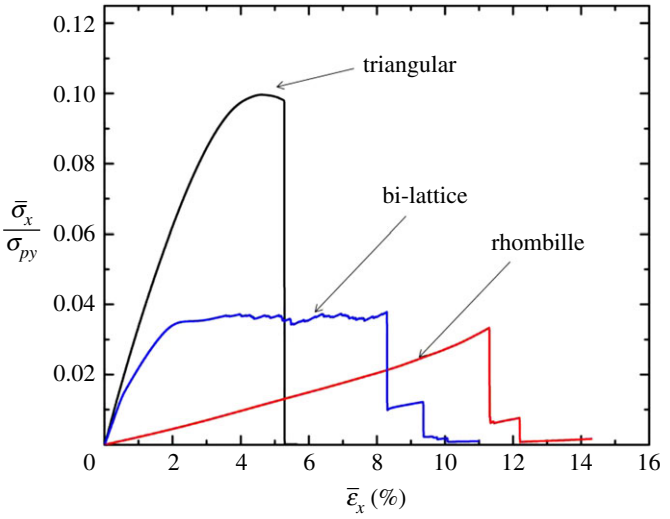


Figure 9. Comparison of the behaviour of triangular, rhombille and bi-lattices. (Online version in colour.)

This description explains how the damage of the separated oblique *ho*-rods is evenly distributed in the material volume. The critical feature of the partially damaged material is that it remains intact and preserves its bearing ability and its stiffness is close to the stiffness in the elastic stage before the damage starts, as is seen from the loading–unloading curves.

A snapshot of the final stage of the evenly distributed damage in the specimen before the macro-crack appears is presented in figure 6*b*, where red points indicate the ruptured rods.

(b) Comparison with homogeneous lattices

To highlight the advantages of the heterogeneous bi-lattice, we compare its stress–strain diagram with the diagrams of two homogeneous lattices with uniform elements.

- The first compared lattice is triangular with the same relative density, $\rho = 0.231$. The thickness of its elements in accordance with (2.1) is $T_r = T_h = T = 0.7$ mm. The comparison presented in figure 9 shows that the Young modulus of the triangular lattice is close to that modulus of the bi-lattice, and the triangular lattice has significantly higher strength. On the other hand, the triangular lattice fails for relatively small deformations and is less efficient at dissipating energy before breaking, as is discussed below.
- The second compared lattice is rhombille; its microstructure is shown in the middle part of figure 1*c*. The specimen for this lattice was obtained by removing the *h*-rods in the bi-lattice; therefore, its relative density is a little smaller, $\rho = 0.198$. Since the obtained lattice becomes bending dominated, its elastic performance drops down by an order of magnitude, which illustrates the importance of the thin rods in the suggested bi-lattice.

The obtained experimental results allow for comparing the energy release before the total failure. We compare the heterogeneous bi-lattice and the homogeneous triangular lattice. The mechanical energy released by a specimen during the experiment is equal to the area below the force–displacement diagram (figure 10*a*,*b*). It is the sum of the elastic strains energy E_{el} and the energy dissipated due to the plastic deformation and the rupture of separate rods E_d

$$E_{\text{tot}} = E_{el} + E_d \tag{4.6}$$

Downloaded from royalsocietypublishing.org/rsta/article-pdf/doi/10.1098/rsta.2019.0107/1316862/rsta.2019.0107.pdf
by University Freiburg user
on 04 November 2026

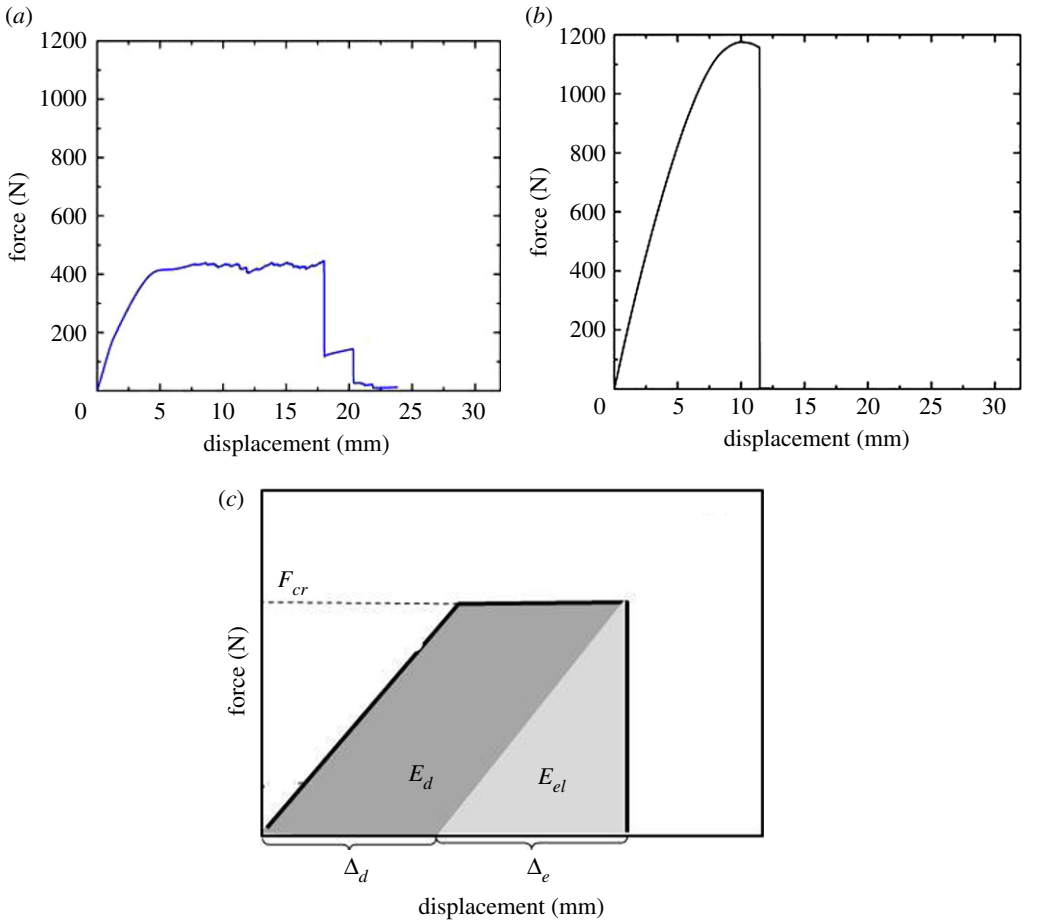


Figure 10. Force versus displacement diagrams for the bi-lattice (*a*), for the triangular lattice (*b*) and the illustration of their structure (*c*).

as is illustrated schematically in figure 10*c*. It is convenient to use this scheme for the further considerations, thus,

$$E_{el} = \tfrac{1}{2} F_{cr} \Delta_e \quad \text{and} \quad E_d = F_{cr} \Delta_d, \tag{4.7}$$

where F_{cr} is the critical force corresponding to the plateau level and defined by the lattice strength, Δ_e and Δ_d are the specimen elongations caused by the elastic and non-elastic deformations, respectively. The approximate experimental values of these quantities for both lattices are derived from the force–displacement diagrams in figure 10*a*,*b* and the ratios of the total and the dissipated energies are

$$\eta_{\text{tot}}^{\text{exp}} = \frac{E_{\text{tot}}^b}{E_{\text{tot}}^t} = 0.66 \tag{4.8}$$

and

$$\eta_d^{\text{exp}} = \frac{E_d^b}{E_d^t} = 1, \tag{4.9}$$

where the superscripts '*b*' and '*t*' denote hereafter the quantities related to the bi-lattice and the triangular lattice, respectively. So the triangular lattice specimen of the same size performs better.

The influence of the specimen length L_x on the above ratios is different. The triangular lattice fails when a crack propagates across the sample, but the bi-lattice tolerates damage uniformly distributed in the whole volume. Therefore, the released energy in the triangular lattice is

Downloaded from royalsocietypublishing.org/rsta/article-pdf/doi/10.1098/rsta.2019.0107/1316862/rsta.2019.0107.pdf
by University Freiburg user
on 04 November 2026

independent of the length of the sample, but the released energy in the bi-lattice linearly grows with the sample length.

The elastic elongations can be expressed through the average strains $\bar{\varepsilon}_x^{(el)}$ corresponding to the limit of the elastic response

$$\Delta_e^b = \bar{\varepsilon}_x^{(el)b} L_x \tag{4.10}$$

and

$$\Delta_e^t = \bar{\varepsilon}_x^{(el)t} L_x. \tag{4.11}$$

The non-elastic displacement of the triangular lattice is caused by the plastic deformation and rupture of the rods along the crack line, consequently, the displacement Δ_d^t is independent of the specimen length. Contrarily, in the bi-lattice the damage is evenly distributed in the material volume, consequently Δ_d^b scales with the element length

$$\Delta_d^b = \alpha L_x. \tag{4.12}$$

Therefore, the energies ratios are

$$\left.\begin{aligned} \eta_{\text{tot}}(L_x) &= \frac{F_{cr}^b(2\alpha + \bar{\varepsilon}_x^{(el)b})}{F_{cr}^t(2\Delta_d^t/L_x + \bar{\varepsilon}_x^{(el)t})} \\ \text{and} \qquad \eta_d(L_x) &= \frac{F_{cr}^b \alpha L_x}{F_{cr}^t \Delta_d^t}. \end{aligned}\right\} \tag{4.13}$$

For a sufficiently long specimen, the bi-lattice has a much higher energy absorbing capacity. Namely, after deriving the values of parameters entering formulae (4.13) from the experimental curves in figure 10 one obtains $\eta_{\text{tot}}(\infty) = 1.5$ and $\eta_d(\infty) \to \infty$.

5. Concluding remarks

The present research is motivated by the previous paper [21] on fault-tolerant beam lattices made of brittle material. The design concept obtained in that work is essentially geometrical: the lattice must be inhomogeneous, which stimulates damage in the weak links; the damage does not propagate due to strong links; therefore, the localized damage occurs in many spots in the lattice. The partially damaged lattice accumulates the damage and releases the impact energy while keeping its stiffness, strength and structural integrity. The concept is robust; it was numerically tested for a elastic-brittle material, and in the present paper, experimentally verifies this concept for a elastic–plastic material and finds consistent results.

We tested the heterogeneous lattice consisting of two types of beams. Thick beams form a rhombille bending-dominated lattice, and thinner beams are added to transform it to a triangular lattice. The thinner beams play an essential role in switching the elastic response from the bending dominated to the stretch dominated. The effective stiffness of the obtained heterogeneous isotropic lattice (bi-lattice) is just 16% less than the stiffness of the uniform triangular lattice; the later has the maximal possible stiffness for the given relative density. On the other hand, the bi-lattice demonstrates the fault-tolerant failure response better than the triangular lattice. Namely, the final stage of localized damage where a catastrophic macro-crack propagates is preceded by a stage of evenly distributed damage of space-separated failed elements.

In addition to the forms of distributed damage for brittle lattices described in [21], the experiments revealed new forms of distributed damage for elastic–plastic materials. For small axial deformation of the specimen, the elastic response of the bi-lattice is linear. Upon greater deformation, groups of thinner elements buckle; after the buckling, the lattice remains linearly elastic with decreased stiffness. Even greater deformation causes plastic yielding followed by the rupture of another group of lattice elements that results in a plateau region at the stress–strain diagram. The loading–unloading curves show that during this stage the lattice remains stiff and preserves its bearing ability. Remarkably, the switch from the linear elastic to the plastic response does not include the external force drop which takes place for the parent material.

Downloaded from royalsocietypublishing.org/rsta/article-pdf/doi/10.1098/rsta.2019.0107/1316862/rsta.2019.0107.pdf
by University Freiburg user
on 04 November 2026

The comparison of the failure of the fault-tolerant inhomogeneous bi-lattice and the homogeneous triangular one shows that the bi-lattice is preferable from the total energy release point of view thanks to the extended stage of evenly distributed damage. Its excellent energy absorption capacity becomes pronounced for the energy irreversibly dissipated by plastic deformation and rupture of lattice elements. Note that the heterogeneous microstructure of the considered bi-lattice with thin h-beams surrounded by thicker r-beams is a discrete analogue of the biocalcite-like composite, characterized by soft inclusions embedded in a stiff matrix. The advantage of such a microstructure for increasing the defect tolerance ability of a composite in the framework of fracture problems was emphasized in [26].

This work investigates distributed damage in fault-tolerant heterogeneous lattices experimentally. The considered bi-lattice is less stiff and less strong than uniform triangular one, but it remains intact for the relatively high deformations, its damage is not catastrophic, and it possesses an excellent energy absorption capacity. Future research will investigate the design of three-dimensional fault-tolerant trusses.

Data accessibility. This article has no additional data.

Authors' contributions. V.S. and S.R. prepared samples and conducted experiments. M.R. and A.C. developed a theory of fault-tolerant lattices and found their optimal parameters; M.R. conducted numerical simulation.

Competing interests. We declare we have no competing interests.

Funding. The authors gratefully acknowledge support by DMS, National Science Foundation, award no. 1515125 and by Israel Science Foundation, grant no. 1494/16. Stephan Rudykh gratefully acknowledges the support of Grainger Institute for Engineering and the University of Wisconsin–Madison.

Appendix A

The effective elastic moduli of the heterogeneous bi-lattice with the microstructure shown in figure 1*b* are given by the following formulae, see [21]

$$\nu_* = \frac{4t_r^2((1-t_r^2)+4t_h^2((1-t_h^2)+t_r^3t_h(1-9t_h^2)+t_rt_h(1+7t_h^2)}{P_1(t_r,t_h)} \tag{A 1}$$

and

$$\frac{E_*}{E_p} = \frac{2(2t_r+t_h)(8t_r^4+9t_rt_h+t_r^3t_h+t_rt_h^3+9t_r^3t_h^3+8t_h^4)}{\sqrt{3}P_1(t_r,t_h)}, \tag{A 2}$$

where

$$t_h = T_h/l, \quad t_r = T_r/l$$

and

$$P_1(t_r,t_h) = 4t_r^2P_2(t_r)+t_rt_h(19+9t_h^2)+(3t_r^3+4{t_h}^2)P_2(t_h),\ P_2(t)=1+3t^2.$$

References

1. Reilly GC, Currey JD. 1999 The development of microcracking and failure in bone depends on the loading mode to which it is adapted. *J. Exp. Biol.* **202**, 543–552.
2. Ziopos P, Currey JD. 1994 The extent of microcracking and the morphology of microcracks in damaged bone. *J. Mater. Sci.* **29**, 978–986. (doi:10.1007/BF00351420)
3. Barthelat F. 2007 Biomimetics for next generation materials. *Phil. Trans. R. Soc. A* **365**, 2907–2919. (doi:10.1098/rsta.2007.0006)
4. Currey J. 2001 Sacrificial bonds heal bone. *Nature* **414**, 699. (doi:10.1038/414699a)
5. Thompson JB, Kindt JH, Drake BHansma, Hansma PK. 2001 Bone indentation recovery time correlates with bond reforming time. *Nature* **414**, 773–776. (doi:10.1038/414773a)
6. Slesarenko V, Kazarinov N, Rudykh S. 2017 Distinct failure modes in bio-inspired 3D-printed staggered composites under non-aligned loadings. *Smart Mater. Struct.* **26**, 035053. (doi:10.1088/1361-665X/aa59eb)
7. Barthelat F. 2014 Designing nacre-like materials for simultaneous stiffness, strength and toughness: optimum materials, composition, microstructure and size. *J. Mech. Phys. Solids* **73**, 22–37. (doi:10.1016/j.jmps.2014.08.008)

Downloaded from royalsocietypublishing.org/rsta/article-pdf/doi/10.1098/rsta.2019.0107/1316862/rsta.2019.0107.pdf
by University Freiburg user
on 04 November 2026

8. Slesarenko V, Volokh KY, Aboudi J, Rudykh S. 2017 Understanding the strength of bioinspired soft composites. *Int. J. Mech. Sci.* **131-132**, 171–178. (doi:10.1016/j.ijmecsci.2017.06.054)
9. Kothari K, Hu Y, Gupta S, Elbanna A. 2018 Mechanical response of two-dimensional polymer networks: role of topology, rate dependence, and damage accumulation. *J. Appl. Mech.* **85**, 031008-1–031008-11. (doi:10.1115/1.4038883)
10. McGugan M, Pereira G, Sorensen BF, Toftegaard H, Branner K. 2015 Damage tolerance and structural monitoring for wind turbine blades open access. *Phil. Trans. R. Soc. A* **373**, 20140077. (doi:10.1098/rsta.2014.0077)
11. Worden K, Farrar CR. 2007 An introduction to structural health monitoring. *Phil. Trans. R. Soc. A* **365**, 303–315. (doi:10.1098/rsta.2006.1938)
12. Cherkaev A, Slepyan L. 1995 Waiting element structures and stability under extension. *Int. J. Damage Mech.* **4**, 58–82. (doi:10.1177/105678959500400104)
13. Cherkaev A, Cherkaev E, Slepyan L. 2005 Transition waves in bistable structures: I. Delocalization of damage. *J. Mech. Phys. Solids* **53**, 383–405. (doi:10.1016/j.jmps.2004.08.002)
14. Slepyan L, Cherkaev A, Cherkaev E. 2005 Transition waves in bistable structures: II. Analytical solution, wave speed, and energy dissipation. *J. Mech. Phys. Solids* **53**, 407–436. (doi:10.1016/j.jmps.2004.08.001)
15. Cherkaev A, Zhornitskaya L. 2004 Dynamics of damage in two-dimensional structures with waiting links. In *Asymptotics, singularities and homogenisation in problems of mechanics* (ed. AB Movchan), pp. 273–284. Dordrecht, the Netherlands: Kluwer.
16. Cherkaev A, Vinogradov V, Leelavanichkul S. 2006 The waves of damage in elastic-plastic lattices with waiting links: design and simulation. *Mech. Mater.* **38**, 748–756. (doi:10.1016/j.mechmat.2005.06.017)
17. Leelavanichkul S, Cherkaev A, Adams D, Solzbacher F. 2009 Energy absorption of a helicoidal bistable structure. *J. Mech. Mater. Struct.* **5**, 305–321. (doi:10.2140/jomms)
18. Cherkaev A, Cherkaev E, Leelavanichkul S. 2011 Principle of optimization of structures against an impact. *J. Phys.: Conf. Ser.* **319**, 1–16. (https://doi.org/10.1088/1742-6596/319/1/012021)
19. Cherkaev A, Leelavanichkul S. 2012 An impact protective structure with bistable links. *Int. J. Damage Mech.* **21**, 697–711. (doi:10.1177/1056789511410458)
20. Cherkaev A, Ryvkin M. 2019 Damage propagation in 2d beam lattices: 1. Uncertainty and assumptions. *Arch. Appl. Mech.* **89**, 485–501. (doi:10.1007/s00419-018-1429-z)
21. Cherkaev A, Ryvkin M. 2019 Damage propagation in 2d beam lattices: 2. Design of an isotropic fault-tolerant lattice. *Arch. Appl. Mech.* **89**, 503–519. (doi:10.1007/s00419-018-1428-0)
22. Lipperman P, Ryvkin M, Fuchs MB. 2007 Nucleation of cracks in two-dimensional periodic cellular materials. *Comput. Mech.* **39**, 127–139. (doi:10.1007/s00466-005-0014-9)
23. Fuchs MB. 2016 *Structures and their analysis*. Switzerland: Springer International Publishing.
24. Ryvkin M, Fuchs MB, Nuller B. 1999 Optimal design of infinite repetitive structures. *Struct. Optim.* **18**, 202–209. (doi:10.1007/BF01195995)
25. Slesarenko V. 2018 Towards mechanical characterization of soft digital materials for multimaterial 3D-printing. *Int. J. Eng. Sci.* **123**, 62–72. (doi:10.1016/j.ijengsci.2017.11.011)
26. Sen D, Buehler MJ. 2011 Structural hierarchies define toughness and defect- tolerance despite simple and mechanically inferior brittle building blocks. *Sci. Rep. (Nature)* **35**, 1–15. (doi:10.1038/srep00035)

Downloaded from royalsocietypublishing.org/rsta/article-pdf/doi/10.1098/rsta.2019.0107/1316862/rsta.2019.0107.pdf
by University Freiburg user
on 04 November 2026